Spatio-Temporal Urban Heat Island Phenomena Assessment using Landsat Imagery: A Case Study of Bangkok Metropolitan and its Vicinity, Thailand

Suwit Ongsomwang*, Songkot Dasananda and Wilawan Prasomsup

School of Remote Sensing, Suranaree University of Technology, Nakhon Ratchasima 30000, Thailand

ARTICLE INFO

Received: 19 Jan 2018
Received in revised:
7 Mar 2018
Accepted: 16 Mar 2018
Published online:
3 Apr 2018
DOI: 10.14456/ennrj.2018.13

Keywords:
Land surface temperature (LST)/ Urban heat island (UHI)/ WAI/ URI/ TGCI/ Bangkok metropolitan and its vicinity (BMV)

*** Corresponding author:**
E-mail: suwit@sut.ac.th

ABSTRACT

Applications of LST data to advanced research on UHI phenomena and its intensity are still relatively low in Thailand. The main objectives of this study are (1) to extract and predict LST data associated with urban and non-urban areas from Landsat imageries and (2) to quantify the intensity of UHI phenomena and its changes over BMV between 2006 and 2026. The research methodology was conducted systematically to extract and predict the LST associated with the urban and non-urban areas in order to assess the intensity of UHI phenomena. The results show that WAI as UHI intensity is extremely critical between 2006 and 2022 and becomes critically severe during 2024 and 2026. The result also show that URI as a degree of UHI development has increased from 2010 to 2016, however, it will suddenly decrease in 2018 and continuously increase between 2020 and 2026. In addition, TGCI analysis indicates that a decreasing temperature trend is dominant in the existing urban areas while an increasing temperature trend shows remarkably in urban expansion areas. These findings confirm the impacts of urbanization and urban development state on UHI intensity. In conclusion, the approaches and results of this study can be applied to master the urban planning properly, especially the mitigation of UHI phenomena in the future.

1. INTRODUCTION

Urban Heat Island (UHI) is a phenomenon whereby urban regions experience warmer temperatures than their rural, undeveloped surroundings (Roth, 2013). This situation is more pronounced in crowded mega cities and has become a key factor in deteriorating the urban ecological environment in these current days. In principle, the level of the UHI intensity is influenced by several associated factors, for examples, local and synoptic weather, season, time of day, city size and its geographical location, urban morphology, and anthropogenic heat (Chang, 2016). To identify UHI strength, near-ground air temperature data at the preferred urban and rural reference sites are needed for the analysis. These data are conventionally accumulated from a set-up network of ground measurements or from remote observation by satellite-based instruments. Among which, the most effective ones are the advanced thermal infrared sensors onboard NASA's Landsat satellites that has routinely operated since 1972 (Landsat 1 to 8). Their continuous measurements can provide comprehensive spatio-temporal characteristics of land surface temperature (LST) over a specific location worldwide at monthly temporal scale (Mendelsohn et al., 2007). These LST data can be applied as input data for determining the near-ground air temperature data needed for the UHI mapping and intensity analysis (Tran et al., 2006; Sukthong, 2008; Dan et al., 2010; Dontree, 2010; Srivanit et al., 2012; Qiao et al., 2014; Fang, 2015; Kikon et al., 2016; Singh et al., 2017; Suwanprasit, 2017; Estoque et al., 2017) including for some other aspects like air quality assessment (Weng and Yang, 2006; Lim et al., 2009; Zheng et al., 2017) or detection/ mapping of active forest fire hotspots (Potapov et al., 2008; Chowdhury and Hassan, 2015; Ongsomwang and Ruthamnong, 2017).

In Thailand, UHI occurrences and their impacts are major concerns, especially on some metropolitan cities like Bangkok (the capital) and Chiang Mai. Considering the prior works on these issues, these mainly rely on the ground-based measurement data whereas applications of satellite-based data for these issues are still rare and limited in scope in these investigations. Also, the intensification of the UHI problem for those cities in the near future has never been systematically quantified and reported so far.

This study aims to provide an overall comprehension of the development and intensity of the UHI phenomena with the prominent indices (e.g., Weighted Average Heat Island Intensity (WAI), Urban Heat Island Ratio Index (URI) and Brightness Temperature Grade Change Index (TGCI) over Bangkok metropolitan and its vicinity over 20 years, from 2006 to 2026. The objectives of this study are (1) to extract and predict LST data associated with urban and non-urban areas from Landsat imageries and (2) to quantify the intensity of UHI phenomena and its change.

2. METHODOLOGY

2.1 Study area

The study area is Bangkok metropolitan and its vicinity (BMV) which consists of Bangkok, Nakhon Pathom, Nonthaburi, Pathum Thani, Sumut Prakan, and Samut Sakhon provinces with total land area of 7,762 km^2 (Figure 1). Basic statistics on land utilization and socio-economic data of BMV is summarized in Table 1. In 2015, Bangkok Metropolitan as the Capital of Thailand has the highest urban and built-up land, number of population, population density, and gross provincial product compared to other provinces. Additionally, Bangkok, Nonthaburi, and Samut Prakan are more urbanized than others and many environmental problems exist in these areas such as air, noise and water pollution and traffic congestion.

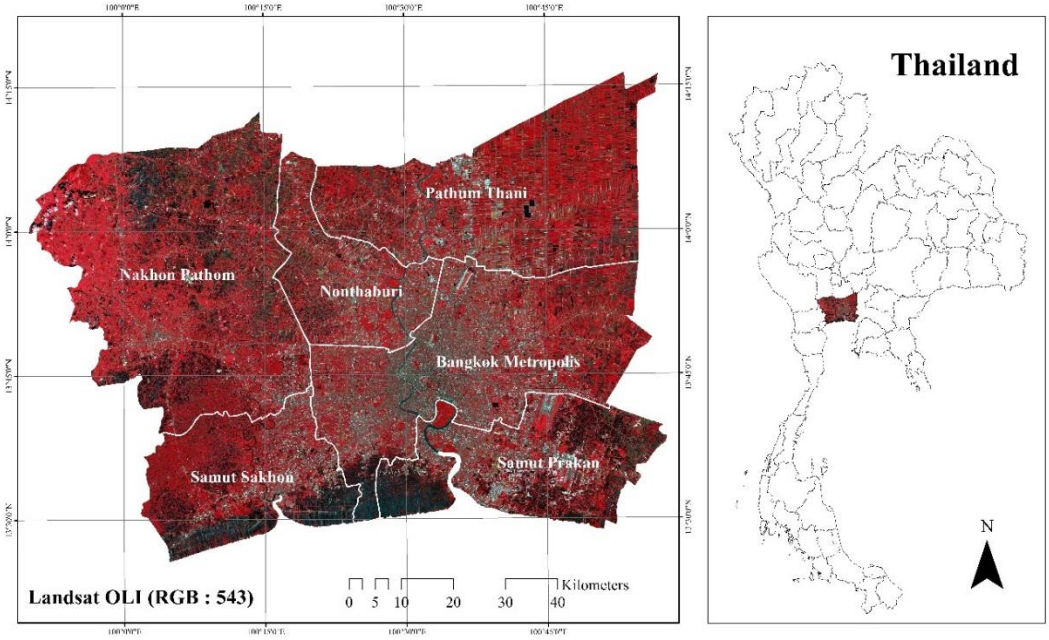

Figure 1. Study area map

Table 1. Basic statistics on land utilization and socio-economic data of Bangkok and its vicinity

Administrative area	Area[1]	Urban and built-up land in 2015[2]		Population[1]		Population density[1]	Gross provincial product[2] (billion baht)	
	(km^2)	(km^2)	(%)	In 1995	In 2015	In 2015	In 1995	In 2015
Bangkok metropolitan	1,568.74	1,054.30	67.21	6,347,250	8,643,230	5,510	1,583.68	4,437.41
Nakhon Pathom	2,168.30	507.46	23.40	740,980	1,039,477	479	81.83	300.22
Nonthaburi	622.3	278.64	44.78	708,853	1,487,317	2,390	60.24	287.69
Pathum Thani	1,525.90	441.38	28.93	547,037	1,447,485	949	168.80	341.82
Samut Prakan	1,004.50	408.37	40.65	931,318	2,016,023	2,007	199.56	685.39
Samut Sakhon	872.3	195.80	22.45	400,058	945,654	1,084	119.38	344.55
BMC	7,762.04	2,885.96	37.18	9,675,496	15,579,186	2,007	2,213.50	6,397.07

[1]Office of the National Economic and Social Development Board (2016)

[2]Land Development Department (2016)

2.2 Research methodology

Research methodology was conducted to assess the UHI phenomena, which derives from three main components, (1) LST extraction and prediction, (2) Urban and non-urban extraction and prediction and (3) Intensity of UHI phenomena assessment (Figure 2).

2.2.1 LST extraction and prediction

The thermal infrared Band 6 of Landsat 5 and 7, and Band 10 of Landsat 8 between 2006 and 2016 were used to extract LST data using Single-Channel method. Considering the result from a study of Wang et al. (2016) , it is clearly shown that the Single-channel method provides a high precision which is able to develop an LST product from Landsat series data. In this study, Landsat imageries with cloud cover less than 10% were first selected and downloaded from the USGS website. Then, digital numbers (DN) from the thermal infrared band of Landsat was converted to LST data under the Model Builder module of ESRI ArcGIS software with the following three steps:

1) Conversion to top of atmosphere (TOA) radiance

The DN data of thermal band were converted to spectral radiance at top of atmosphere (TOA) using the radiance scaling factors provided in the metadata file (USGS, 2016) as:

$$L_\lambda = M_L Q_{cal} + A_L \quad (1)$$

where, L_λ is TOA spectral radiance (watts/m^2 srad μm) , M_L is band specific multiplicative rescaling factor from the metadata, A_L is band specific additive rescaling factor from the metadata and Q_{cal} is quantized and calibrated standard product DNs.

2) Conversion to at-satellite BT

The obtained spectral radiance data at TOA were further converted to brightness temperature (*BT*) based on uniform emissivity (ε) assumption using Equation. 2 (USGS, 2016).

$$BT = \frac{K_2}{ln(\frac{K_1}{L_\lambda}+1)} \quad (2)$$

where, *BT* is at-satellite BT in Kelvin (K) , L_λ is TOA spectral radiance (watts/m^2 ster μm), K_1 and K_2 is band specific thermal conversion from the metadata file (Table 2).

3) Correction for spectral emissivity

The *BT* values obtained above were referenced to a black body with ε of 1. Therefore, correction of land surface emissivity (ε) was necessary according to the nature of land cover. Thus, the LST data with emissivity correction were estimated using Equation 3 as suggested by Artis and Carnahan (1982).

$$LST = \frac{BT}{1+(\lambda \cdot BT/\rho)ln\varepsilon} \quad (3)$$

Here, λ is wavelength of emitted radiance, ρ is the formulated constant (1.438×10^{-2} m K) and ε is land surface emissivity that was estimated using NDVI Thresholds method as suggested by Sobrino et al. (2004) and Jeevalakshmi et al. (2017).

After that, the extracted LST data between 2002 and 2016 were further refined using simple linear analysis based on their relationships with in situ mean temperature of eight Thai Meteorological Department (TMD) stations as suggested by Jensen (2007). The refined LST data were then further used to extrapolate LST data between 2018 and 2026 by Trend function of MS Excel spreadsheet and Image conversion function of ERDAS Imagine software.

Table 2. Thermal constant of K_1, K_2 value

Thermal constant	Landsat 8		Landsat 7	Landsat 5
	Band 10	Band 11	Band 4	Band 6
K_1	774.89	480.89	666.09	607.76
K_2	1,321.08	1,201.14	1,282.71	1,260.56

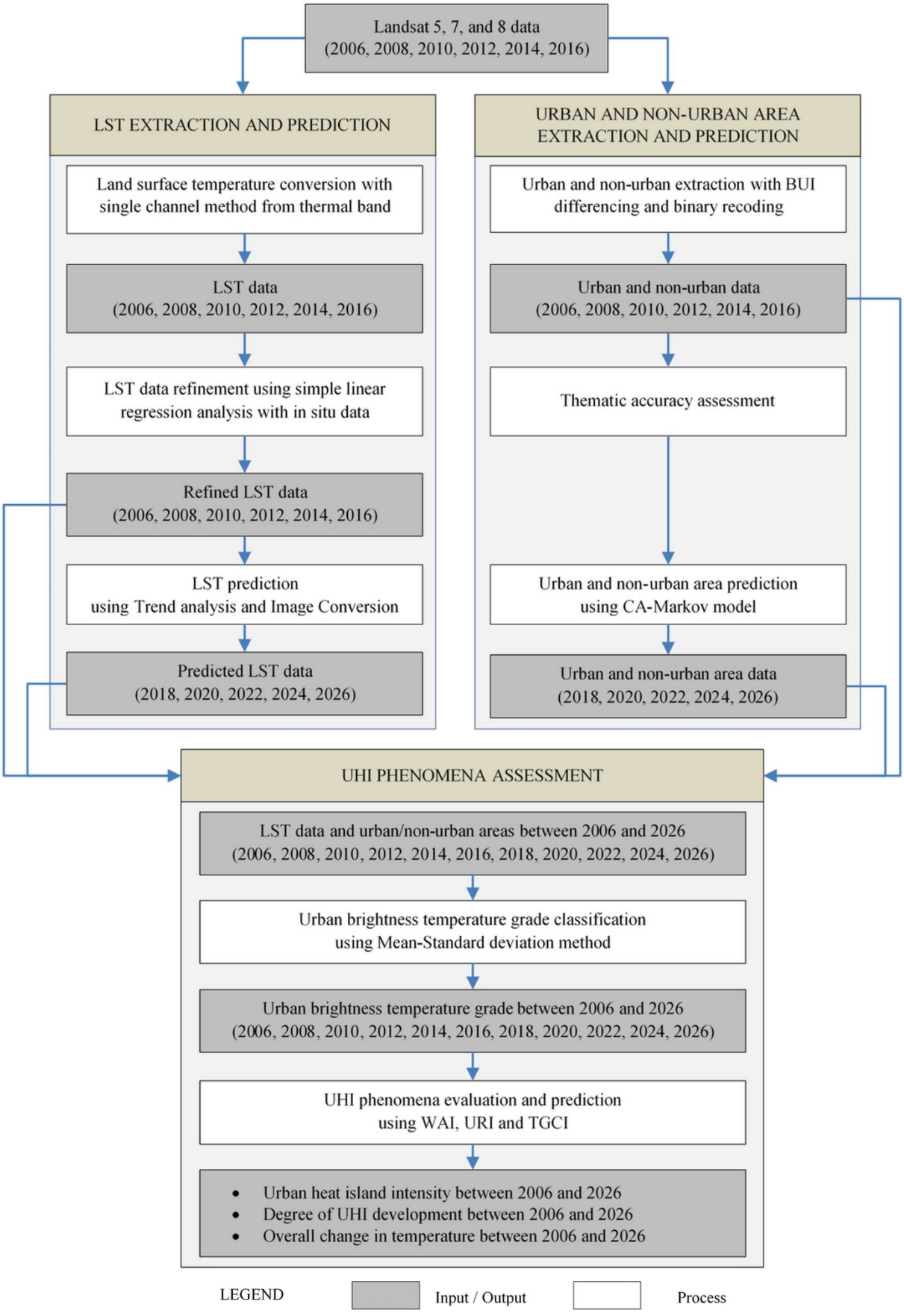

Figure 2. Workflow of research methodology

2.2.2 Urban and non-urban area extraction and prediction

The refined LST data between 2006 and 2016 were used to calculate NDBI and NDVI and their results were then applied to calculate built-up index (BUI) using Equation 4 as suggested by Zha et al. (2003).

$$\text{Built-up index (BUI)} = \text{NDBI} - \text{NDVI} \quad (4)$$

where, NDBI is Normalized Difference Built-up Index [(SWIR-NIR) / (SWIR+ NIR)] and NDVI is Normalized Difference Vegetation Index [(NIR-RED) / (NIR+RED)].

In this study, urban areas (city, town, commercial, village, institutional, transportation, communication and utilities, industrial land and bare land) and non-urban areas (agricultural land, forest land and parks, and water bodies) were classified using BUI differencing and binary recoding (Table 3). He et al. (2010) stated that the BUI had improved universality and provided lower commission error for urban and non-urban areas extraction compared with original method (NDBI and NDVI).

Table 3. Pixel value of representative land covers after differencing and binary recoding

Indices	Urban areas	Non-urban areas		
		Agriculture land	Forest land and parks	Water bodies
NDVI	0	1	1	0
NDBI	1	1 or 0	1 or 0	0
NDBI-NDVI	1	0 or 1	0 or 1	0

In addition, accuracy assessment of the derived urban and non-urban maps was also determined using reference data from very high spatial resolution imageries of Google Earth website. In this case, 426 sample points were applied based on binomial probability theory (Fitzpatrick-Lins, 1980) with the expected accuracy of 80% and the acceptable error of sampling of 5% and stratified random sampling.

The derived urban and non-urban areas between 2006 and 2016 were further applied to predict urban and non-urban areas between 2018 and 2026 using CA-Markov model. In principle, the model uses Markov chain matrix to determine the quantity of change and cellular automata (CA) to spatially allocate land use and land cover (LULC) changes (Paegelow and Olmedo, 2005). CA-Markov model has been frequently applied to predict LULC change and urban growth such as Kamusoko et al. (2009), Ongsomwang and Saravisutra (2011), Sang et al. (2011), and Adhikari and Southworth (2012).

2.2.3 Intensity of UHI phenomena assessment

1) Urban brightness temperature grade classification

Before temperature grade classification, the extracted and predicted LST data between 2006 and 2026 were normalized (0 to 1) to eliminate the impact of the imaging time and make the UHI effect more comparable (Fang, 2015) as:

$$N = \frac{T_i - T_{Min}}{T_{Max} - T_{Min}} \quad (5)$$

where, N is the result value after normalizing, T_i is the original BT value, $T_{\min}$ is the minimum value of BT, and $T_{\max}$ is the maximum value of BT.

These normalized LST data in urban areas were further classified into 5 classes of the defined brightness temperature grade (BTG) based on Mean (μ) and Standard deviation (σ) values as suggested by Xu et al. (2011) as follows:

(1) Low temperature area: $LST < \mu - \sigma$

(2) Secondary low temperature area: $\mu - \sigma \leq LST < \mu - 0.5\sigma$

(3) Medium temperature area: $\mu - 0.5\sigma \leq LST < \mu + 0.5\sigma$

(4) Secondary high temperature area: $\mu + 0.5\sigma \leq LST \leq \mu + \sigma$

(5) High temperature area: $LST > \mu + \sigma$

2) UHI intensity assessment

To quantify intensity of UHI phenomena over BMV between 2006 and 2026, three different UHI indices included WAI, URI and TGCI were selected for the analysis.

The WAI describes UHI intensity by sum of products between the different five grade temperatures in built-up areas with average temperature in outskirt areas and percent of temperature grade areas (Dan et al., 2010) as:

$$WAI = \sum_{i=1}^{5} (T_{iavg} - T_{oavg}) \times A_i \quad (6)$$

where, T_{iavg} represents average temperature of different BTG from high to low respectively, T_{oavg} is the average temperature in outskirt area, and A_i represents the percentage of different BTG from high to low.

Meanwhile, the URI, which is used to depict development degree of heat island, was also extracted using Equation 7 as suggested by Xu and Chen (2004).

$$URI = \frac{1}{100m} \sum_{i=1}^{n} w_i \cdot p_i \quad (7)$$

where, m is the number of BTG, i represents BTG that in urban region is higher than in suburbs, n is the number of BTG that in urban region is higher than in suburbs, w is weighted value, it takes the value of BTG as result, and p is area percentage.

In addition, the TGCI that reflects the overall change in either decreasing or increasing temperature was extracted based on transition matrix of BTG between two dates as detailed in Equation 8 (Xu et al., 2011) as:

$$TGCI = \sum_{i=1}^{n} w_i \times GB_i \quad (8)$$

where, n is the number of BTG change types that has twenty-five types in theory, GB is grade change series of temperature brightness and w is the area percentage. If the grade change becomes decreasing, the GB will be negative. In contrast, if the grade change becomes increasing, the GB will be positive.

3. RESULTS AND DISCUSSION

3.1 LST extraction between 2006 and 2016

Table 4 presents simple linear regressions analysis for LST data refinement based on in situ mean temperature of TMD data. These results indicate notably high positive correlation with the coefficient (R) varying between 0.8424 (in 2012) and 0.9357 (in 2006).

Table 4. List of simple linear equations for refinement of LST data

No	Equation	R	R^2	Landsat series and date
1	Y = 0.9022X +3.1222	0.9357	0.8756	Landsat 5, 1 January 2006
2	Y = 0.8454X +4.1313	0.9308	0.8663	Landsat 7, 9 January 2008
3	Y = 0.9567X +1.5897	0.9230	0.8520	Landsat 7, 14 November 2010
4	Y = 0.4383X +16.74	0.8424	0.7096	Landsat 7, 21 February 2012
5	Y = 0.6643X +9.9818	0.9078	0.8241	Landsat 8, 17 November 2014
6	Y = 0.6643X +11.017	0.9239	0.8535	Landsat 8, 12 April 2016

X is mean temperature of TMD (independent variable) and Y is extracted LST (dependent variable).

These discovered equations were then used to modify LST data as statistical results shown in Table 5. It is obvious that LST in 2016, acquired on 12th April 2016, shows the highest average LST, while LST in 2010, acquired on 14th November 2010, shows the lowest average LST. As expected, the highest average LST occurring in April is related to the hottest month of summer season, yet mid-October to mid-February is winter season (TMD, 2015). This confirms the impact of season changes on temperature accurately.

In addition, Figure 3 shows an example of the refined LST data distribution in 2014 (winter season). It is found that the highest temperature class (29.86 - 36.45°C) mostly appears in central business district (CBD) of BMV, particularly Bangkok while the lowest temperature class (17.14 - 25.39°C) distributes in agricultural areas of Nakhon Pathom and Samut Sakhon.

Table 5. Basic statistical data of modified LST data between 2006 and 2016

Month	Year	LST (°C)			
		Minimum	Maximum	Mean	Standard deviation
January	2006	21.00	39.48	27.56	2.12
January	2008	21.01	40.74	26.51	1.70
November	2010	19.01	31.81	23.24	1.57
February	2012	21.02	38.23	27.16	2.09
November	2014	17.14	36.46	27.08	1.83
April	2016	21.23	42.33	32.35	2.06

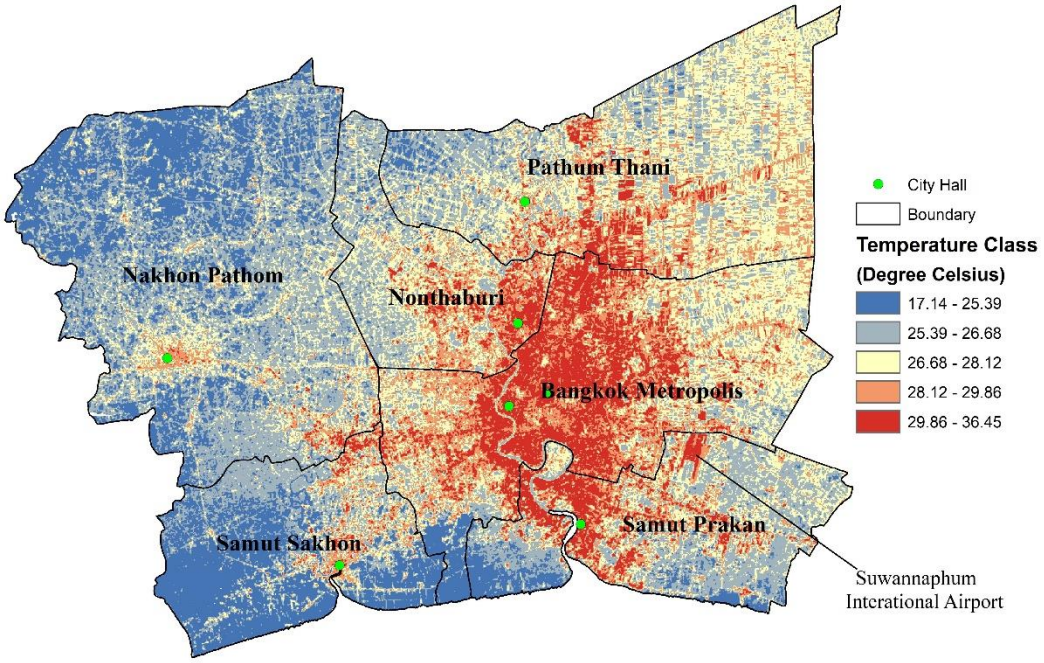

Figure 3. Distribution of refined LST data in 2014

3.2 LST prediction between 2018 and 2026

The basic statistical data of the predicted LST data between 2018 and 2026 from the extrapolation with Trend Analysis technique is presented in Table 6. From the results, the maximum predicted LST continuously increases from year to year, however the minimum predicted LST continuously decreases in these periods. According to the Trend function of MS Excel, it calculates the linear trend line (either negative or positive relationship) through a given set of LST array. Nevertheless, the mean LST prediction over BMV tends to increase in the future. The predicted mean temperatures seem to rise slowly from around 27.81°C (in 2018) to 29.96°C (in 2026) which is not greatly different from those observed in the past (as seen in Table 5).

Table 6. Basic statistical data of predicted LST data between 2018 and 2026

Year	LST (°C)			
	Minimum	Maximum	Mean	Standard deviation
2018	17.63	40.13	27.81	1.79
2020	15.38	42.95	28.35	1.94
2022	12.90	45.77	28.88	2.11
2024	10.41	48.58	29.42	2.30
2026	7.92	51.40	29.96	2.50

3.3 Urban and non-urban area extraction between 2006 and 2016

Area and percentage of urban and non-urban areas extraction between 2006 and 2016 using BUI differencing and binary recoding (see Table 3) are summarized in Table 7. The results show the continuous increase of urban area from 1,735.64 km^2 (22.68%) in 2006 to 2,895.61 km^2 (37.83%) in 2016, with annually increasing rate of 116 km^2. In terms of the credibility, these classified maps were achieved by considering the relatively high overall accuracy of 81.46% (2006), 85.21% (2008), 87.56% (2010), 87.79% (2012), 88.97% (2014), and 91.08% (2016), respectively. The discovered accuracy levels of this study are corresponding with a previous work of Zha et al. (2003), who applied BUI for urban and non-urban area extraction in Nan Jing, China with the overall accuracy of 92.60%.

Figure 4 demonstrates urban and non-urban distribution in 2014 for the BMV where the highest proportion of the classified urban areas (about 52%) appear in Bangkok as expected, while Samut Sakhon contains the lowest urban percentage (about 33%).

Table 7. Area and percentage of urban and non-urban area between 2006 and 2016

Year	Area in km^2			Area in percent		
	Urban	Non-urban	Total	Urban	Non-urban	Total
2006	1,735.64	5,918.65	7,654.29	22.68	77.32	100
2008	2,038.75	5,615.54	7,654.29	26.64	73.36	100
2010	2,209.45	5,444.84	7,654.29	28.87	71.13	100
2012	2,379.52	5,274.77	7,654.29	31.09	68.91	100
2014	2,638.47	5,015.82	7,654.29	34.47	65.53	100
2016	2,895.61	4,758.68	7,654.29	37.83	62.17	100

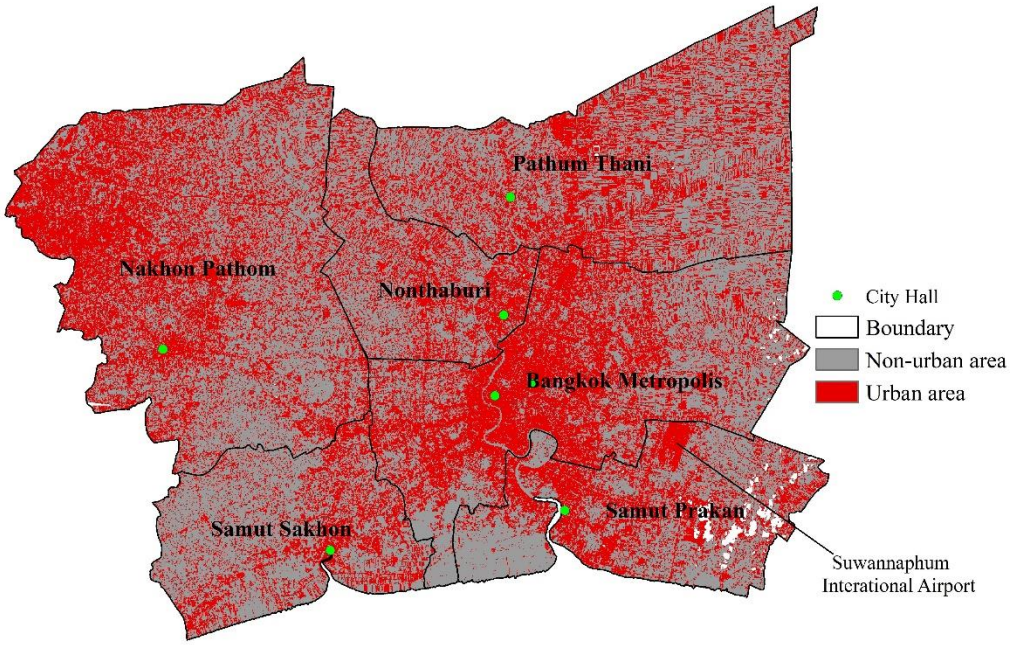

Figure 4. Distribution of urban and non-urban in BMV in 2014

3.4 Urban and non-urban area prediction between 2018 and 2026

Considering the results of urban and non-urban area prediction between 2018 and 2026 in Table 8, they also esimate that the urban area will expand from 3,139.58 km^2 (41.02%) in 2018 to 3,828.25 km^2 (50.01%) in 2026, with an annual increase of 116.58 km^2. In theory, the size of the urban portion can influence UHI intensity outcome (Chang, 2016), therefore overall intensity of the UHI phenomena over the BMV in the near future should be more pronounced in general.

Table 8. Area and percentage of urban and non-urban area between 2006 and 2026

Year	Area in km^2			Area in percent		
	Urban	Non-urban	Total	Urban	Non-urban	Total
2018	3,139.58	4,514.71	7,654.29	41.02	58.98	100
2020	3,361.20	4,293.09	7,654.29	43.91	56.09	100
2022	3,495.29	4,159.00	7,654.29	45.66	54.34	100
2024	3,621.76	4,032.53	7,654.29	47.32	52.68	100
2026	3,828.25	3,826.04	7,654.29	50.01	49.99	100

3.5. Spatial analysis between LST and urban and non-urban areas

Regarding the result from zonal operation technique in spatial analysis of LST data associated with urban/non-urban areas between 2006 and 2026, it appears that the mean temperature in urban areas are higher than those of non-urban areas by 1-2°C (Table 9) in all years. Figure 5 illustrates two transect-temperature profiles of BMV along both N-S and W-E directions showing variation of LST data in relation to the corresponding land cover type in 2014. These temperature profiles are compared with forest land at Bang Krachao of Samut Prakan, used as a reference area. Similar to the previous finding, it is confirmed that average temperature in urban areas are noticeably higher than those of the non-urban ones, such as rivers, lakes, forests, parks, and agriculture. In addition, UHI phenomena along Transect No. 1 appears at distances of 2,500 to 8,750 m, 12,500 to 20,000 m and 28,750 to 32,500 m by a notable increase of the urban temperature compared with the surrounding temperature (Figure 5 (c)). Likewise, UHI phenomena occur at distance of 0 to 24,000 m and 28,000 to 31,300 m along Transect No. 2 (Figure 5 (d)).

Table 9. LST data of urban and non-urban area between 2006 and 2026

Year	LST in urban area (°C)			LST in non-urban area (°C)		
	Minimum	Maximum	Mean	Minimum	Maximum	Mean
2006	21.00	39.48	29.66	21.01	39.41	26.94
2008	21.01	36.57	27.88	21.08	40.74	26.00
2010	19.02	31.81	24.24	19.25	31.51	22.83
2012	21.02	38.16	28.49	21.02	38.23	26.55
2014	17.14	36.46	27.97	18.19	35.88	26.61
2016	22.85	42.33	33.10	21.23	42.08	31.89
2018	17.63	40.13	28.59	20.76	35.17	27.26
2020	15.38	42.95	29.12	20.30	36.95	27.73
2022	12.90	45.77	29.64	19.65	38.74	28.24
2024	10.41	48.58	30.19	19.00	40.61	28.72
2026	7.92	51.40	30.74	18.82	42.31	29.17

3. 6 Brightness temperature grade classification and UHI phenomena evaluation

Results of BTG classification in urban areas between 2006 and 2026 are displayed in Figure 6 which clearly shows that distributing pattern of the classified BTG varies from year to year due to the changes on mean and standard deviation values of LST. For example, BTG class in CBD of Bangkok in 2014 measures as a high temperature class, however it becomes a medium temperature class in 2016. (See Figure 6 (e) and 6 (f)). In addition, it should be noted that the limitation of valid Landsat data due to cloud cover shall directly affect LST derivation as well as the BTG classification. Ideally, Landsat imagery for BTG classification should be acquired on anniversary dates to ensure seasonal agreement of temperature conditions among multi-dates data implementation (Jensen, 2007).

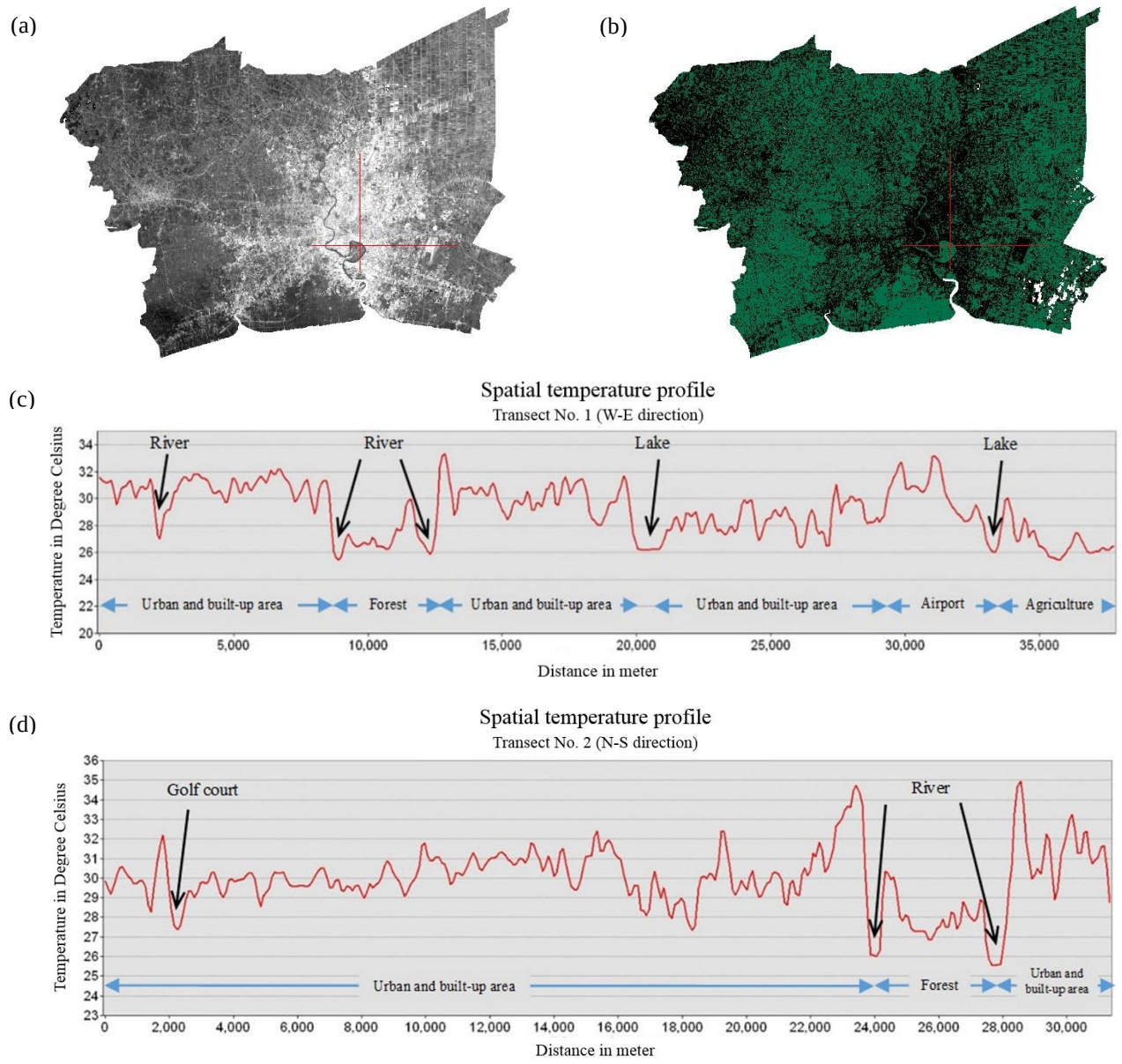

Figure 5. Temperature profiles along transect lines in (a) N-S direction (b) W-E direction with urban and non-areas in 2014

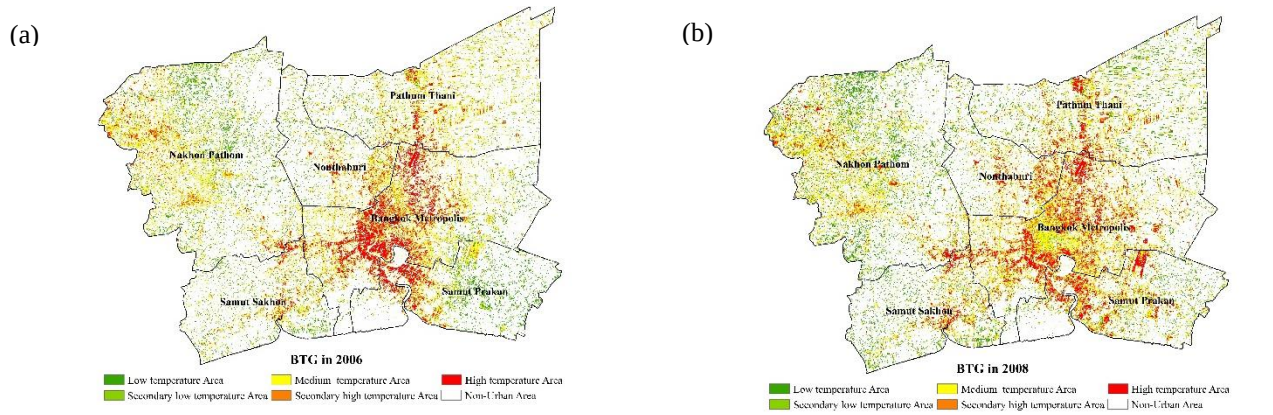

Figure 6. Distribution spatio-temporal patterns of BTG classification: (a) 2006, (b) 2008, (c) 2010, (d) 2012, (e) 2014, (f) 2016, (g) 2018, (h) 2020, (i) 2022, (j) 2024, and (k) 2026.

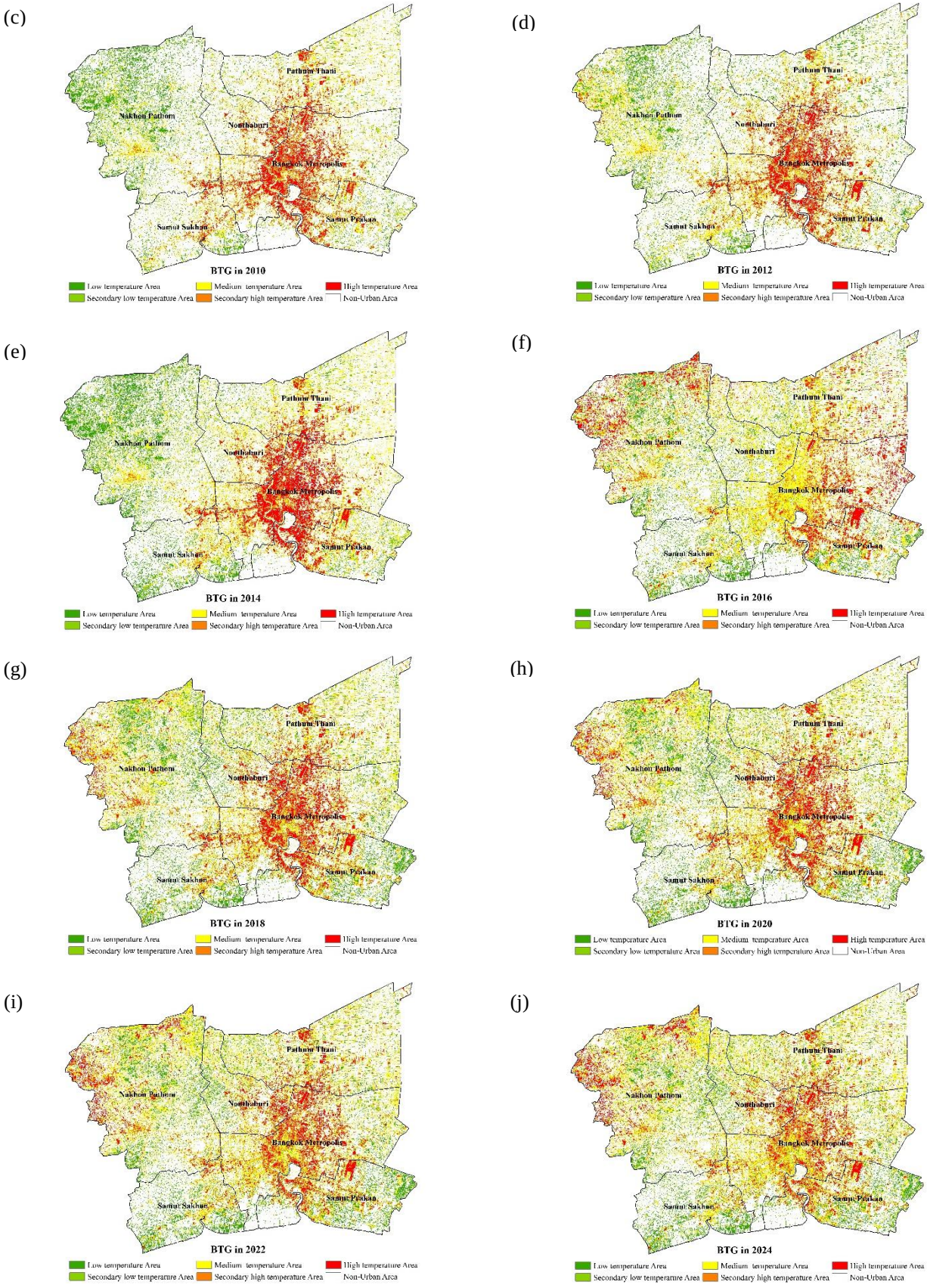

Figure 6. Distribution spatio-temporal patterns of BTG classification: (a) 2006, (b) 2008, (c) 2010, (d) 2012, (e) 2014, (f) 2016, (g) 2018, (h) 2020, (i) 2022, (j) 2024, and (k) 2026. (cont.)

(k)

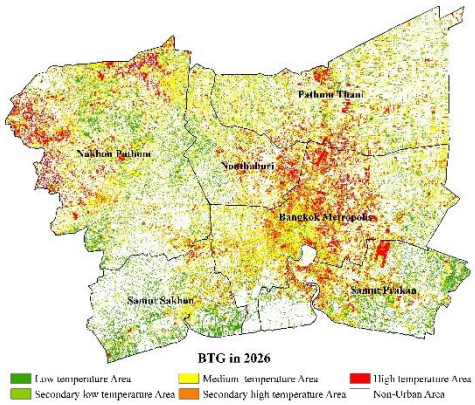

Figure 6. Distribution spatio-temporal patterns of BTG classification: (a) 2006, (b) 2008, (c) 2010, (d) 2012, (e) 2014, (f) 2016, (g) 2018, (h) 2020, (i) 2022, (j) 2024, and (k) 2026. (cont.)

3.7 UHI intensity and its severity

The UHI intensity analysis using WAI index shows that WAI values continuously decrease from 2006 to 2016 except in 2010 and 2016 and gradually decrease from 2018 to 2026 (Figure 7). Regarding the UHI intensity classification given by Dan et al. (2010), the result of this study shows the extremely critical severity of UHI intensity (WAI > 3°C) between 2006 and 2022. Also, the UHI intensity is predicted to be critically severe from 2024 to 2026 (2°C < WAI ≤ 3°C). However, it should be noted that since WAI is calculated based on the average of five grade temperature classes in urban areas, the average temperature of outskirt areas, and proportional areas of five grade temperature classes in urban areas (see detail in Equation 6), the trend of the observed WAI in the future will decrease the same as the outskirt areas, whereas urban areas will increase. This observation can be confirmed by using simple linear regression analysis (Figure 8) showing a highly negative relationship between WAI and total urban area ($R^2 = 0.9509$).

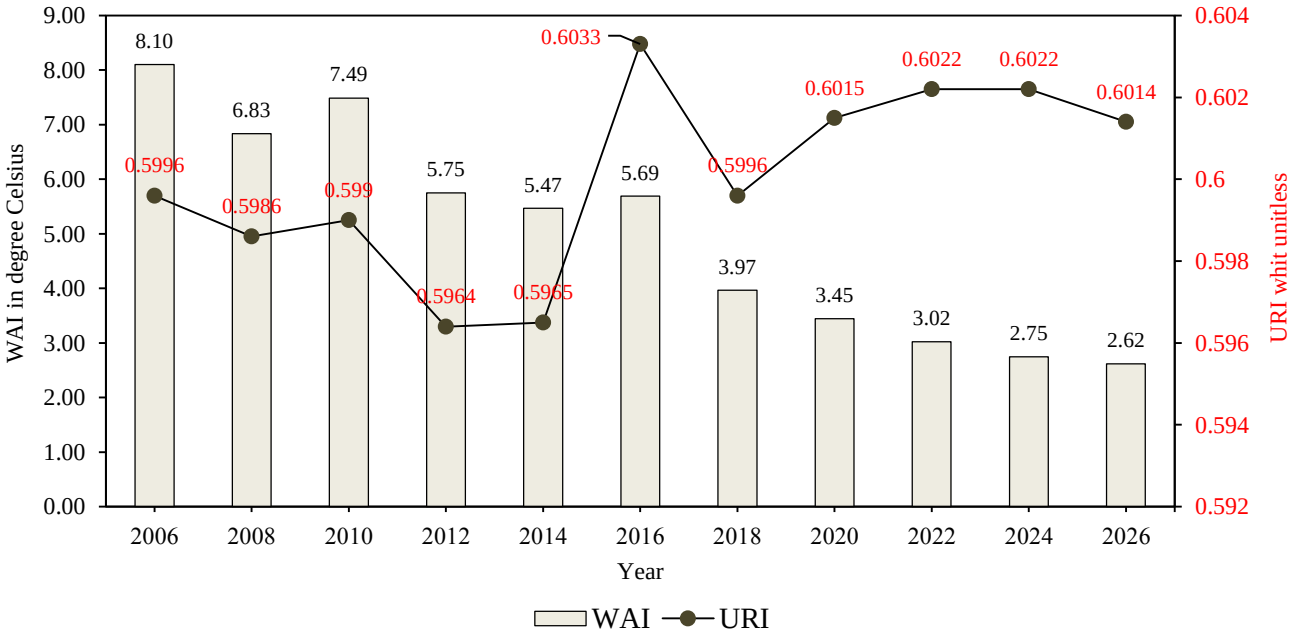

Figure 7. Dynamic change of WAI and URI between 2006 and 2026

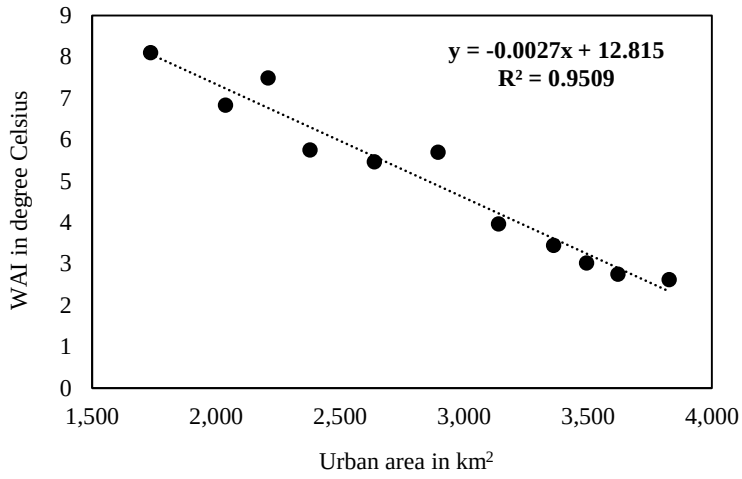

Figure 8. Relationship between urban area and WAI

In the meantime, more fluctuations can be seen in URI data profile with a downward trend from 2006 to 2014 followed by a rapid rise to the highest temperature in 2016 and sudden drop in 2018. The rising trend is eventually observed to continue from 2018 onward. This finding shows the increment of UHI development in the future. A larger URI indicates a stronger UHI effect.

Qiao et al. (2014) mentioned that URI was in high correlation with the urban land area since proportional area of five grade temperature classes in urban area was applied for URI calculation (see detail in Equation 7) . However, the relationship between urban areas and URI values in this current study shows low positive correlation with R^2 as 0.3795 (Figure 9). The possible reason might be the negative influence of several outliers inherent in URI data.

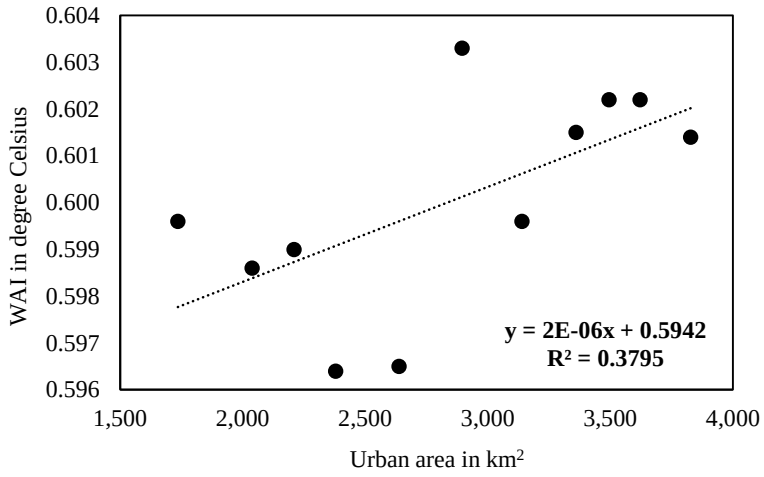

Figure 9. Relationship between urban area and URI

3.8 Overall change in temperature

The TGCI values for overall BTG changes in existing urban and urban expansion areas from 2006 to 2026 are presented in Table 10. As seen in the results, decreasing trends of TGCI in the "existing urban areas" are found in most years, except from 2010 to 2012 and 2016 to 2018. As for a reason, these two periods demonstrate the slightly increasing UHI intensity. On contrary, increasing trends of TGCI in the "urban expansion areas" are dominant in most years, except from 2020 to 2022. The increasing trend in these urban expansion areas may imply that UHI intensity shall increase due to the process of urbanization which gradually expands from the city center to the outskirt area.

Table 10. TGCI of overall change in temperature in old urban and urban expansion areas

Period	TGCI value change in	
	Old urban areas	Expansion urban areas
2006-2008	-0.159	0.586
2008-2010	-0.272	0.607
2010-2012	0.043	0.648
2012-2014	-0.158	0.591
2014-2016	-0.076	1.572
2016-2018	0.051	0.196
2018-2020	-0.023	0.038
2020-2022	-0.027	-0.016
2022-2024	-0.030	0.023
2024-2026	0.000	0.015

4. CONCLUSIONS

Spatio-temporal UHI phenomena assessment and its intensity over BMV from 2006 to 2026 is successfully implemented using three key indices (WAI, URI and TGCI) based on the extracted and predicted LST data associated with urban and non-urban areas. It can be concluded that the average temperature varies from around 23°C in 2010 to around 32°C in 2016. In the meantime, urban area is predicted to continuously increase from 1,735. 64 km^2 in 2006 to 3,828.25 km^2 in 2026.

It can be concluded that the trend of the observed WAI will decrease corresponding with the outskirt area whereas the urban area will increase in contrary regarding the highly negative relationship between WAI and total urban area from simple linear regression analysis. In the meantime, more fluctuations are seen in URI data profiles which indicate the increment of UHI development in the future, however, the relationship between urban areas and URI shows a low positive correlation. The TGCI analysis indicates a decreasing trend is dominant in the existing urban areas while an increasing trend is prominent in most years within the urban expansion areas. These findings show the influence of urbanization and urban development on UHI intensity.

Eventually, it can be suggested that the results of this research can be applied to either assist or master the urban planning mission in order to mitigate the effect of UHI phenomena in the future. Particularly, areas with increased WAI class and high URI may require more practical plans to reduce UHI intensity such as urban green space and green architecture design.

ACKNOWLEDGEMENTS

Financial and facility supports from Suranaree University of Technology (SUT) are gratefully acknowledged by the authors. Authors wish to thank Dr. Pantip Piyatadsananon, SUT for her valuable comments and suggestions for improvement the manuscript.

REFERENCES

Adhikari A, Southworth J. Simulating forest cover changes of Bannerghatta National Park based on a CA-Markov model: a remote sensing approach. Remote Sensing 2012;4:3215-43.

Artis DA, Carnahan WH. Survey of emissivity variability in thermography of urban areas. Remote Sensing of Environment 1982;12(4):313-29.

Chang HT. A temporal and spatial analysis of urban heat island in basin city utilizing remote sensing techniques. Proceeding of the International Archives of the Photogrammetry, Remote Sensing and Spatial Information Sciences; 2016 July 12-19; Prague, Czech Republic; 2016.

Chowdhury EH, Hassan QK. Operational perspective of remote sensing-based forest fire danger forecasting systems. ISPRS Journal of Photogrammetry and Remote Sensing 2015;104:224-36.

Dan S, Xu H, Xue W, He J, Dan B. Comparison and analysis of research methods for urban heat island effects based on Landsat TM6. Proceedings of 2010 Second IITA International Conference on Geoscience and Remote Sensing; 2010 Aug 28-31; Qingdao: China; 2010.

Dontree S. Relation of land surface temperature (LST) and land use/land cover (LULC) from remotely sensed data in Chiang Mai-Lamphun Basin. Proceeding of the SEAGA Conference; 2010 Nov 23-26; Hanoi, Vietnam; 2010.

Estoque RC, Murayama Y, Myint SW. Effects of landscape composition and pattern on land surface temperature: an urban heat island study in the megacities of Southeast Asia. Science of the Total Environment 2017;577:349-59.

Fang G. Prediction and analysis of urban heat island effect in Dangshan by remote sensing. International Journal on Smart Sensing and Intelligent Systems 2015;8(4): 2195-211.

Fitzpatrick-Lins K. The Accuracy of Selected Land Use and Land Cover Maps at Scales of 1: 250,000 and 1:100,000. U.S. Govt. Print. Off.; 1980.

He C, Shi P, Xie D, Zhao Y. Improving the normalized difference built-up index to map urban built-up areas

using a semiautomatic segmentation approach. Remote Sensing Letters 2010;1(4):213-21.

Jeevalakshmi D, Narayana Reddy S, Manikiam B. Land surface temperature retrieval from LANDSAT data using emissivity estimation. International Journal of Applied Engineering Research 2017;12(20):9679-87.

Jensen JR. Remote Sensing of the Environment: An Earth Resource Perspective. 2nd ed. New Jersey: United States: Pearson Prentice Hall; 2017.

Kamusoko C, Aniya M, Adi B, Manjoro M. Rural sustainability under threat in Zimbabwe - Simulation of future land use/cover changes in the Bindura district based on the Markov-cellular automata model. Applied Geography 2009;29:435-47.

Kikon N, Singh P, Singh SK, Vyas A. Assessment of urban heat islands (UHI) of Noida city, India using multi-temporal satellite data. Sustainable Cities and Society 2016;22:19-28.

Land Development Department. Land Use Data in Thailand: Land Use in the Central Region. [Internet]. 2016 [cited 2018 Mar 5]. Available from: http://www1.ldd.go.th/WEB_OLP/report_research_C.html

Lim HS, MatJafri MZ, Abdullah K, Wong CJ. Air pollution determination using remote sensing technique. In: Jedlovec G, editor. Advances in Geoscience and Remote Sensing. InTech: Croatia; 2009. p. 71-92.

Mendelsohn R, Kurukulasuriya P, Basist A, Kogan F, Williams C. Climate analysis with satellite versus weather station data. Climatic Change 2007;81:71-83.

Office of the National Economic and Social Development Board. [Internet]. 2016 [cited 2018 Mar 5]. Available from:http://www.nesdb.go.th/nesdb_en/more_news.php?cid= 156&filename=index.

Ongsomwang S, Ruthamnong S. Burned area assessment using BAMS: a case study of upper northern region, Thailand. Suranaree Journal of Science and Technology 2017;24(3):327-42.

Ongsomwang S, Saravisutra A. Optimum predictive model for urban growth prediction. Suranaree Journal of Science and Technology 2011;18(2):141-52.

Paegelow M, Olmedo MTC. Possibilities and limits of prospective GIS land cover modelling-a compared case study: Garrotxes (France) and Alta Alpujarra Granadina (Spain). International Journal of Geographical Information Science 2005;19(6):697-722.

Potapov P, Hansen MC, Stehman SV, Loveland TR, Pittman K. Combining MODIS and landsat imagery to estimate and map boreal forest cover loss. Remote Sensing of Environment 2008;112:3708-19.

Qiao Z, Tian T, Zhang L, Xu X. Influences of urban expansion on urban heat island in Beijing during 1989-2010. Advances in Meteorology 2014;2014:11.

Roth M. Urban heat islands. In: Fernando HJS, editor. Handbook of environmental fluid dynamics Volume 2: Systems, Pollution, Modeling, and Measurements. New York: Taylor & Francis Group; 2013. p. 143-59.

Sang L, Zhang C, Yang J, Zhu D, Yun W. Simulation of land use spatial pattern of towns and villages based on CA-Markov model. Mathematical and Computer Modelling 2011;54:938-43.

Singh P, Kikon N, Verma P. Impact of land use change and urbanization on urban heat islands in Lucknow city, central India: a remote sensing based estimate. Sustainable Cities and Society 2017;32:100-14.

Sobrino JA, Jiménez-Munˇoz JC, Paolini L. Land surface temperature retrieval from LANDSAT TM 5. Remote Sensing of Environment 2004;90:434-40.

Srivanit M, Kazunori H, Vivarad P. Assessing the impact of urbanization on urban thermal environment: a case study of Bangkok metropolitan. International. Journal of Applied Science and Technology 2012;2(7):243-56.

Sukthong P. Thermal Remote Sensing Application on Urban Heat Island Case Study: Pathumthani Urban Areas. [Dissertation]. Thammasat University; 2008.

Suwanprasit C. Pattern of land-use change and urban heat island during 20 years in Chiang Mai, Thailand. Proceedings of 17th the International Multidisciplinary Scientific Geo Conference; 2017 June 29 - July 5; Albena: Bulgaria; 2017.

Thai Meteorological Department (TMD). The Climate of Thailand. [Internet]. 2015 [cited 2016 Dec 15] . Available from: https://www.tmd.go.th/en/archive/thailand_climate.pdf

Tran H, Uchihama D, Ochi S, Yasuoka Y. Assessment with satellite data of the urban heat island effects in Asian mega cities. International Journal of Applied Earth Observation and Geoinformation 2006;8(1):34-48.

United States Geological Survey (USGS). Landsat 8 (L8) data user handbook [Internet]. 2016 [cited 2016 Jan 14]. Available from: http://landsat.usgs.gov/documents/Landsat8 DataUsers Handbook.pdf.

Wang M, Zhang Z, He G, Wang G, Long T, Peng Y. An enhanced single-channel algorithm for retrieving land surface temperature from Landsat series data. Journal of Geophysical Research: Atmospheres 2016;121(19): 11,712-22.

Weng Q, Yang S. Urban air pollution patterns, land use, and thermal landscape: an examination of the linkage using GIS. Environmental Monitoring and Assessment 2006;117:463-89.

Xu H, Chen Y, Dan S, Qiu W. Dynamical monitoring and evaluation methods to urban heat island effects based on RS&GIS. Procedia Environmental Sciences 2011;10:1228-37.

Xu HQ, Chen, BQ. Remote sensing of the urban heat island and its changes in Xiamen City of SE China. Journal of Environmental Science 2004;16:276-81.

Zha Y, Gao J, Ni S. Use of normalized difference built-up index in automatically mapping urban areas from TM imagery. International Journal of Remote Sensing 2003;24(3):583-94.

Zheng S, Zhou X, Singh RP, Wu Y, Ye Y, Wu C. The spatiotemporal distribution of air pollutants and their relationship with land-use patterns in Hangzhou city, China. Atmosphere 2017;8(6):110.